Published online 4 September 2012

Nucleic Acids Research, 2013, Vol. 41, No. 1 ***e12***
doi:10.1093/nar/gks837

Quantifying RNA–protein interactions *in situ* using modified-MTRIPs and proximity ligation

Jeenah Jung, Aaron W. Lifland, Chiara Zurla, Eric J. Alonas and Philip J. Santangelo*

Wallace H. Coulter Department of Biomedical Engineering, Georgia Institute of Technology and Emory University, 313 Ferst Drive, UA Whitaker Bldg, Atlanta, GA, 30332, USA

Received May 4, 2012; Revised July 18, 2012; Accepted August 12, 2012

ABSTRACT

The stabilization, translation and degradation of RNA are regulated by interactions between *trans*-acting factors, such as microRNA and RNA-binding proteins (RBP). In order to investigate the relationships between these events and their significance, a method that detects the localization of these interactions within a single cell, as well as their variability across a cell population, is needed. To visualize and quantify RNA–protein interactions *in situ*, we developed a proximity ligation assay (PLA) that combined peptide-modified, multiply-labelled tetravalent RNA imaging probes (MTRIPs), targeted to sequences near RBP binding sites, with proximity ligation and rolling circle amplification (RCA). Using this method, we detected and quantified, with single-interaction sensitivity, the localization and frequency of interactions of the human respiratory syncytial virus (hRSV) nucleocapsid protein (N) with viral genomic RNA (gRNA). We also described the effects of actinomycin D (actD) on the interactions of HuR with β-actin mRNA and with poly(A)+ mRNA at both native and increased HuR expression levels.

INTRODUCTION

RNA-binding proteins (RBP) and small RNAs regulate the splicing (1), stability (2), localization (3) and translation (4) of RNA through their interactions with specific *cis*-acting elements within the target RNA sequence. These post-transcriptional regulatory mechanisms play an important role in viral infections (5) and diseases, such as cancer (6,7) and metabolic disease (8). Numerous RBPs and their multiple target sites have been identified and studied using immunoprecipitation and microarray analysis (9). However, biochemical techniques cannot provide the localization or variability of these interactions on a per cell basis. The spatiotemporal organization (3,10) and the population heterogeneity (11) of RNA–protein interactions reflect their functional role in the cell's response to their extracellular environment or internal stimuli via intracellular or intercellular signalling.

Imaging techniques, such as fluorescence resonance energy transfer (FRET) (12,13) and fluorescence complementation (FC) (14), have been used to study RNA–protein interactions. In these methods, the RNA is labelled with either SytoxOrange or the MS2 system. Although the Sytox system is bright, it lacks RNA specificity. In comparison, the MS2-based approach is specific but suffers from limited sensitivity for detecting RNA–protein interactions and lacks the ability to detect these interactions at native levels, requiring expression of the RNA and RBP. To image and quantify native RNA and RNA–protein interactions simultaneously *in situ*, we developed a proximity ligation assay (PLA) that combines peptide-modified, multiply-labelled tetravalent RNA imaging probes (MTRIPs), which enabled sequence-specific imaging of native RNA (15), with proximity ligation and rolling circle amplification (RCA) that allowed the localization of interactions with single-interaction sensitivity (15,16).

Using this assay, we quantified interactions between previously characterized RBPs and either viral or endogenous RNAs, and also investigated changes in such interactions under different experimental conditions. We demonstrated that interactions between the human respiratory syncytial virus (hRSV) nucleocapsid protein (N) and viral genomic RNA (gRNA) increased as the duration of the infection increased. We also imaged and quantified interactions between poly(A)+ mRNA (17) and β-actin mRNA (18) and an RBP, HuR, whose interactions with mRNAs have been implicated in tumourigenesis (19–21). HuR binds to the poly(A) tail (22) and the 3′-untranslated region (3′-UTR) of many genes, including β-actin (23–25). Although predominately within the nucleus, HuR has been shown to shuttle between the nucleus and the cytoplasm through its nucleocytoplasmic shuttling domain, when cells are exposed to specific stimuli, such as actinomycin D (actD) (26), and to stabilize mRNA in the cytoplasm (27,28). We used PLA to examine changes in the HuR–mRNA interactions with native or

*To whom correspondence should be addressed. Tel: +1 404 385 2116; Fax: +1 404 894 4243; Email: philip.santangelo@bme.gatech.edu

overexpressed HuR during transcription inhibition using actD (29). Although we observed cell-to-cell variability in the amount of HuR and mRNA, as well as in the frequency of their interactions, HuR–mRNA interactions generally increased as the amount of HuR increased in the cytoplasm, whereas the amount of mRNA decreased with actD exposure. One clear advantage of this methodology is that it allowed us to quantify the cell-to-cell variability in RNA expression and interactions simultaneously, which is challenging with other methods.

MATERIALS AND METHODS

FMTRIP synthesis

Flag-tagged neutravidin was synthesized by first conjugating flag tag-hyNic (Solulink) to neutravidin (Thermo) modified with 4FB (Solulink) using the manufacturer's protocol. The concentration of flag tag-hyNic and 4FB-modified neutravidin were adjusted to produce molar ratio (MR) of 1-2 flag/neutravidin. After flag labelling, FMTRIPs were assembled as previously described (15). Briefly, 2′-*O*-methyl RNA–DNA oligonucleotide chimeras were designed with a 5′-biotin and dT-C6-NH2 internal modifications (Biosearch Technologies). Cy3B-NHS ester fluorophores (GE Healthcare) were conjugated to the oligonucleotide amine groups using the manufacturer's protocol. Free dye was removed using 3 kD Amicon spin columns (Millipore). The purified, labelled oligonucleotides were then tetramerized by incubation for 1 h at RT with flag-tagged neutravidin at molar ratio of 5:1. The FMTRIP targeting different mRNA sequences (Supplementary Table S23) were assembled separately prior to delivery. Each neutravidin, tetramerized oligonucleotides that target the same sequence. For example, in order to deliver 20 nM FMTRIP for each of three targets in β-actin 3′-UTR, 20 nM FMTRIP was incubated with 100 nM fluorophore-labelled oligonucleotide that encodes one of three sequences. Free ligands were removed using 30 kD Amicon spin columns (Millipore). Three 20 nM FMTRIP, each neutravidin bound to four of the same oligonucleotide sequences, were combined to form a 60 nM FMTRIP mixture.

Cell lines and virus

Vero cells (American Type Culture Collection [ATCC] CCL-81), A549 lung carcinoma cells (ATCC CCL-185) and HeLa cells (ATCC CCL-2) were maintained in High Glucose Dulbecco's modified Eagle's medium (DMEM) (Lonza) with 10% FBS (Hyclone), 100 U/ml penicillin (Invitrogen) and 100 μg/ml streptomycin (Invitrogen). Cells were plated on No 1.5 glass coverslips (Ted Pella) 1 day prior to infection, transfection or imaging.

Virus infection

hRSV A2 strain (ATCC VR-1544) prepared in HEp-2 cells (ATCC CCL-23) at a titer of 1×10^6 plaque forming units ml^{-1}. All cells were infected at >80% confluence, by removing the media, washing with PBS (without Ca^{2+} and Mg^{2+}) and then adding virus at a multiplicity of infection (MOI) of 1 to the cells for 1 h at 37°C. After adsorption, fresh medium was added to the inoculum.

Cell transfection

Cells were transfected using Lipofectamine 2000 Transfection Reagent (Invitrogen) according to the manufacturer's protocol. For each well in a 24-well plate, Vero cells were transfected with 1.0 μg of N-GFP plasmid (a gift from Dr James E. Crowe Jr, Vanderbilt Univ.) and 2 μl Lipofectamine 2000. After 36 h of transfection, FMTRIPs were delivered into cells. For experiments using c-Myc 3′-UTR plasmids, Vero cells were transfected with 0.8 μg GFP-c-Myc plasmid and 1.6 μl Lipofectamine 2000, and 0.4 μg of HuR-GFP plasmid and 0.8 μl Lipofectamine 2000 (the plasmids were gifts from Dr Myriam Gorospe, NIH/NIA). After 48 h of transfection, FMTRIPs were delivered into cells. HeLa cells were transfected with 0.4 μg of HuR-GFP plasmid (a gift from Dr Myriam Gorospe, NIH/NIA) and 0.8 μl Lipofectamine 2000. After 36 h of transfection, FMTRIPs were delivered into cells. For siRNA transfections, HeLa cells were transfected with 200 nM On-TARGETplus Non-targeting siRNA #1 or On-TARGET SMARTpool HuR siRNA (Thermo Scientific Dharmacon) and 1 μl Lipofectamine 2000. After 48 h of transfection, FMTRIPs were delivered into cells.

Probe delivery

For probe delivery, cells were washed in Dulbecco's phosphate buffered saline (DPBS) without $Ca^{2+}$and Mg^{2+} (Lonza), and then incubated with 0.2 U/ml activated SLO (Sigma) in OptiMEM (Invitrogen) containing FMTRIP [30nM, 60 nM or 20nM flag-tagged neutravidin targeted to hRSV, poly(A) or each of 3 β-actin 3′-UTR, respectively] for 10 min at 37°C. Delivery media were replaced with growth media for 15 min to restore membrane integrity before actD exposure or fixation. For studying hRSV infection, FMTRIPs with a 1 flag MR were used, unless otherwise specified. For experiments investigating HuR–mRNA interactions in HeLa cells, FMTRIPs with a 2 MR were used to maximize the signal.

Act D exposure

Cells were incubated for 0.5, 30 and 60 min at 37°C with 5 μg/ml actD (Sigma) in growth medium and fixed at the end of exposure.

Proximity ligation assay

After probe delivery and recovery, cells were fixed with 1% paraformaldehyde (Electron Microscopy Science) in PBS for 10 min, permeabilized using 0.2% Triton X-100 (Sigma) for 5 min and blocked for 1 h with the standard Duolink II blocking solution (Olink Bioscience) or a modified blocking solution, which consists of 0.5% Tween-20 (CalBioChem), 0.1% Triton X-100, 0.1% gelatin (Aurion), 2% donkey serum (VWR) and 1% bovine serum albumin (BSA) (EMD) in PBS. Cells

were washed with PBS for 5 min. Then they were incubated for 30 min at 37°C in each of two primary antibodies (Ab) diluted in 0.25% gelatin, 0.5% Triton X-100, 0.5% donkey serum and 1% BSA in PBS and then corresponding oligonucleotide-labelled PLA probes (Olink Bioscience) diluted in 0.05% Tween-20 in PBS. They were washed with Duolink wash solution (Olink Bioscience) after each Ab incubation. The ligation and RCA reactions (Olink Bioscience) were performed as instructed in the manufacturer's protocol. Then the cells were immunostained or DAPI-stained (Invitrogen) and mounted on slides using Prolong (Invitrogen).

Antibodies

Primary antibodies used were mouse monoclonal anti-flag (1:500 for immunofluorescence (IF), 1:1000 for PLA, Sigma), rabbit polyclonal anti-flag (1:500 for IF, 1:1000 for PLA, Sigma), mouse monoclonal anti-hRSV N (1:500, Abcam), mouse monoclonal anti-hRSV P (1:200 for IF, a gift from Dr James E. Crowe Jr, Vanderbilt Univ.), mouse monoclonal anti-HuR 3A2 (1:6000 for PLA, Santa Cruz), mouse monoclonal anti-HuR 19F12 (1:200 for IF, Santa Cruz) and mouse monoclonal anti-vimentin (1:50 for IF, Developmental Studies Hybridoma Bank). Rabbit polyclonal anti-flag Ab (Sigma) was used unless otherwise specified.

Fluorescence imaging

Unless specified otherwise, all the images were taken using a laser scanning confocal microscope, Zeiss LSM 510 Meta using a 63×, NA 1.4 Plan-Apochromat objective. Resolution was set to 1024 × 1024. Files were imported into Volocity and linearly contrast enhanced for display. Widefield images were taken on an Axiovert 200 M microscope (Zeiss) with a 63× numerical aperture (NA) 1.4 Plan-Apochromat objective, and an ORCA-ER AG camera (Hamamatsu). The imaging was performed using the Volocity acquisition software (PerkinElmer). Image stacks were recorded at 200 nm intervals to adequately sample volumes for iterative deconvolution.

Image processing and analysis

Widefield images were deconvolved using Volocity's deconvolution algorithms. FMTRIP and PLA signal quantification, intensity quantification, as well as Mander's and Pearson's coefficients were computed in Volocity and imported into Excel (Microsoft) or Sigma Plot (Systat) for further analysis and plotting. Images presented have been linearly contrast enhanced for clarity. All calculations were performed directly on raw, deconvolved widefield data or raw confocal data.

Image quantification

The volume of RNA and the PLA frequency/RNA volume were measured using Volocity. Each cell was analysed individually as follows. Each cell was identified by MTRIP signal or vimentin immunostaining. The RNA volume was determined based on the SD intensity. The PLA signal initially was identified as PLA objects by their SD intensity, then separated into individual punctae using the 'separate touching objects' tool. The objects were further filtered based on size and maximum intensity. For each experiment, we analysed at least 30 representative cells; experiments were repeated at least twice. In Sigma Plot, Mann–Whitney rank sum test was used to compare FMTRIP volume and the Pearson's and Manders' coefficients; one-way and two-way ANOVA statistical tests were performed to compare PLA frequency. For one-way ANOVA test, multiple pairwise comparisons were performed with Dunn's method for unequal number of samples and Tukey method for equal number of samples. For two-way ANOVA test, multiple pairwise comparisons were performed with Holm–Sidak.

Quantitative reverse transcriptase polymerase chain reaction

HeLa cells were grown on six-well plates and transfected as described with 2 μg of HuR-GFP plasmid per well. After 36 h post-transfection, they were exposed to actD. At the end of the exposure, total RNA was extracted at the indicated time points using the PARIS kit (Ambion). Total RNA was quantified via UV-VIS spectroscopy. A quantity of 1 μg total RNA was used for cDNA synthesis using the RT^2 first strand kit (SA biosciences) according to the manufacturer's instructions. About 1 μl of the product then was used for Quantitative reverse transcriptase polymerase chain reaction (qRT–PCR) using the Real-time RT^2 qPCR primer assay (SYBR green) in the presence of gene-specific primers for ACTB and 18S rRNA (SA Biosciences). qRT–PCR was performed with three replicates using ABI StepOnePlus real-time PCR system (Applied Biosciences). The relative quantification (RQ) of gene expression and comparative threshold cycle (C_T) values were obtained using an ABI StepOnePlus real-time PCR system. The values were compared with the untransfected cells with no actD exposure. Here, 18S rRNA was used as the internal control (Student's *t*-test: $P = 0.0995$). These values and their summary statistics were used to compare the effects of actD exposure in the transfected and untransfected groups (30). Two-way ANOVA test was performed using the summary statistics provided, and the Bonferroni *post-hoc* method was used to compare the groups.

RESULTS

MTRIPs can be tagged with varying molar ratios of flag peptide

In order to modify MTRIPs for PLA compatibility, we synthesized Cy3B-labelled flag-tagged MTRIPs (FMTRIPs) with a molar ratio (MR) of 1 or 2 flag (Figure 1A), delivered them into live cells using streptolysin O (SLO) (Figure 1B) and post-hybridization, fixed the cells. FMTRIPs were designed against specific RNA sequences near RBP binding sites. The flag peptides on FMTRIPs provided a partner for a PLA reaction with an RBP. Live-cell hybridization and subsequent fixation obviated the need for antigenicity-reducing formamide, allowing for efficient antibody binding.

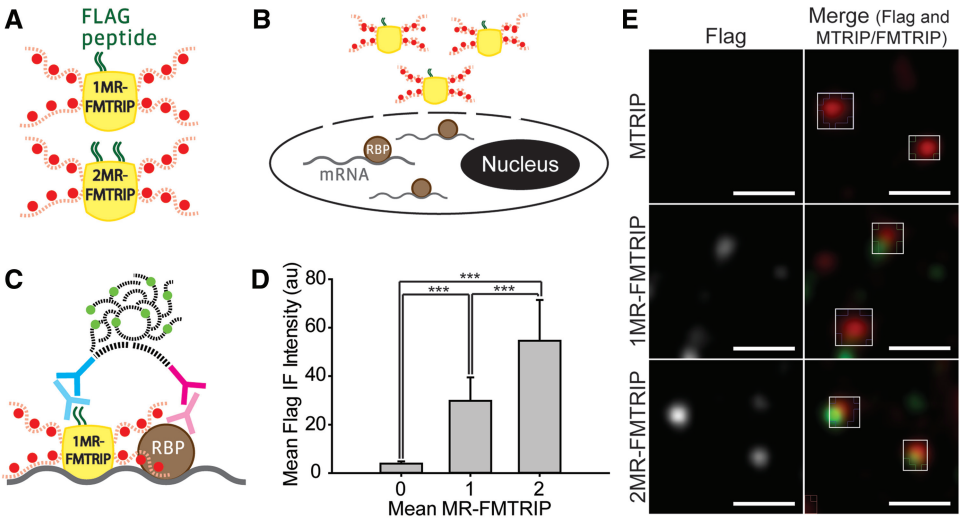

Figure 1. Production and imaging of flag-tagged MTRIP (FMTRIP). (**A**) Flags (dark green) bind to a neutravidin (yellow) with Cy3B-conjugated (red) oligonucleotides to form a 1 or 2 MR-FMTRIP. (**B**) FMTRIPs enter cells via streptolysin O (SLO). (**C**) Antibodies (Ab) (light blue and magenta) and proximity probes (dark blue and magenta) attach to FMTRIP and RBP (brown) on the mRNA (grey); probes join to synthesize a Cy5-equivalent hybridized product (light green) via RCA. (**D**) Comparison of the mean flag immunofluorescence (IF) intensity for 0 (n = 511, mean = 4, SD = 1), 1 (n = 3255, mean = 30, SD = 10) and 2 (n = 4724, mean = 55, SD = 17) MR-FMTRIP. (**E**) Untagged MTRIP, as well as 1 and 2MR-FMTRIP flag IF were imaged using a widefield microscope. MTRIP and FMTRIP (red) and flag IF (green) are merged. Scale bar, 2 µm. a.u., arbitrary units. Error bars, standard deviation.

Anti-flag and anti-RBP Abs were then added to the cells, followed by oligonucleotide-linked proximity probes. If the RNA and protein interacted [<40 nm apart (16)], the oligonucleotides on the proximity probes came together to form a template for a circularized DNA strand by enzymatic ligation. Catalysed by the phi29 DNA polymerase, one of proximity probe's oligonucleotides served as a primer for RCA, whereas three mismatched exonuclease-resistant 2′-*O*-methyl RNA nucleotides at the 3′-end prevented the other proximity probe's oligonucleotide from acting as a primer. This reaction resulted in a coiled single-stranded DNA, the PLA product, complementary to the circular DNA strand and covalently bound to the antibody–antigen complex. The PLA product was detectable by hybridizing complementary Cy5 equivalent-labelled oligonucleotides (Figure 1C) (16).

To confirm the detection of the flag on FMTRIPs, we adsorbed FMTRIPs on glass and immunostained for flag (Figure 1E). The flag immunofluorescence (IF) intensity of FMTRIP with a 2 molar ratio of flag (2MR-FMTRIP) was twice that of 1MR-FMTRIP (Figure 1D). IF was minimal using untagged MTRIPs (Figure 1D and E). An alternate primary anti-Flag Ab showed similar results (Supplementary Figure S1). Using FMTRIPs targeting the hRSV gRNA in infected Vero and A549 cells, we characterized the FMTRIP and flag IF signals by their co-localization with a known RBP, the N protein. Because N binds tightly to gRNA (31), it was expected and confirmed that FMTRIP-labelled gRNA and N immunostaining co-localized (Supplementary Figure S2). In A549 cells fixed 48 h post-infection (PI), the mean flag IF intensity increased with increasing flag MR, as observed on glass (Supplementary Figure S3A and B). The mean Pearson's and Manders' coefficients between flag and gRNA exceeded 0.9, indicating that, when bound to gRNA, the flag on FMTRIP remained on the neutravidin and was accessible to its Ab (Supplementary Figure S3C). We detected no difference between MTRIP- and FMTRIP-labelled gRNA (Supplementary Figure S3A). Vero cells showed similar results (data not shown).

PLA frequency increases with increasing flag molar ratio

To determine the effect of flag valency, PLA was performed between flag and N in hRSV-infected, FMTRIP-delivered A549 cells. We assumed a PLA product, a micron-sized fluorescent puncta, as an occurrence of interaction between N and gRNA (Supplementary Figure S4), and that the volume of objects visualized by FMTRIPs correlated with the RNA copy number (18). A PLA product appeared as a puncta of consistent size and intensity for a variety of analytes, Ab and cell lines (Figure 1D and Supplementary Figure S4), therefore facilitating quantification. At 12 h PI, the mean PLA frequency (number of PLA punctae/FMTRIP volume) increased with more flag (Figure 2), whereas the mean FMTRIP volume remained similar (one-way ANOVA with Dunn's method, $P = 0.326$). No PLA signal was observed using untagged-MTRIP (Figure 2). Likely, not every antibody bound to FMTRIP participated in PLA productively. As PLA detects interactions present at the time of fixation, we likely detected only a subset of gRNA and N that were bound at that moment. The distance between N and flag Ab may exceed the distance limit for proximity ligation due to their conformation or steric hindrance during virus replication. In the case of 2MR-FMTRIP, the second flag Ab might interfere with the probe binding or ligation. Indeed, for 3MR-FMTRIP, the mean flag IF intensity, as well as the mean PLA frequency decreased below those of 1MR (data not

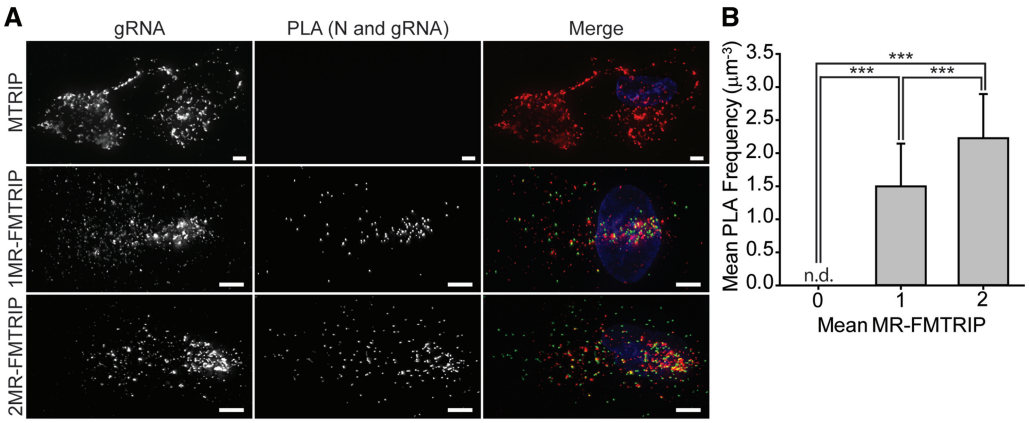

Figure 2. Imaging and quantification of hRSV gRNA FMTRIP and PLA with varying flag molar ratio. (**A**) gRNA FMTRIP and PLA in A549 cells 12 h PI were imaged with a widefield microscope and deconvolved. gRNA (red), PLA (green) and nuclei (blue) are merged. Scale bar, 5 µm. (**B**) Comparison of the mean PLA frequency for 0 ($n = 20$, mean = 0, SD = 0), 1 ($n = 31$, mean = 1.5, SD = 0.6) and 2 ($n = 32$, mean = 2.2, SD = 0.7) MR-FMTRIP in hRSV-infected A549 cells 12 h PI imaged using a widefield microscope. ***$P < 0.001$ (one-way ANOVA with Dunn's method. n.d., not detected. Error bars, standard deviation.

shown), possibly due to steric hindrance by the additional flags and their Ab or quenching by the additional fluorophores.

Optimal blocking is important in achieving high specificity

For accurate RNA–protein PLA, where the RNA is in low abundance, optimal blocking and antibody titration are crucial. The standard Duolink II blocking solution (Olink Bioscience, Sweden) (std) resulted in non-specific signal; modifying it (mod) eliminated the background signal (Supplementary Figure S5). Limiting non-specific Ab binding through titration with untagged-MTRIPs as a negative control helped increase the signal-to-noise ratio. With varying N dilution, the mean PLA frequency fluctuated (Supplementary Figure S6). At low concentrations, the sensitivity decreased, resulting in greater variance; at high concentrations, the specificity decreased, resulting in smaller variance but greater non-specific signal (Supplementary Figure 6B). For each experiment, we optimized the Ab dilution to achieve the highest specificity and minimum assay variance.

hRSV N and gRNA interactions can be imaged and quantified by PLA

Utilizing 1MR-FMTRIPs and PLA, we imaged and quantified hRSV gRNA–N interactions at different times PI (Figure 3). We also immunostained the hRSV phosphoprotein (P) post-PLA to localize nucleocapsids, as hRSV P binds to N in nucleocapsids and as monomers (31). The PLA punctae co-localized with gRNA and P, indicating interactions between gRNA and N (Figure 3A). The frequency of PLA signal increased concomitantly with the duration of infection from 6 to 48 h in both Vero (Figure 3B) and A549 cells (Figure 3C and Supplementary Figure S7). The standard deviation (SD) reflects the heterogeneity in FMTRIP volume and PLA frequency (Figure 3B and C). Untagged MTRIP, N Ab omission and mock-infection controls revealed no PLA signal (Figure 3A). In addition, we observed no interaction between N and gRNA FMTRIPs in Vero cells transfected with the fusion protein, N-GFP, but not infected with hRSV, (Supplementary Figure S8). When N and FMTRIP are present in the cell, without the viral gRNA, they were limited to random interactions, resulting in minimal PLA signal. Hence, we conclude PLA specifically detects interactions between hRSV gRNA and N.

HuR-mRNA interactions can be imaged and quantified by PLA

To further test the specificity of this method, we examined interactions between an RBP, HuR and plasmid-derived mRNAs in the presence and absence of the HuR-binding site, as well as with varying levels of HuR. We used GFP reporter constructs expressing RNA that spanned the GFP coding region and the c-Myc 3′-UTR (referred to as c-Myc) to express GFP with the HuR binding site (c-Myc AB) and without (c-Myc A) in Vero cells (32). The 3′-UTR A segment precedes the HuR binding site in the B segment (32). We designed FMTRIPs to target three sites on this c-Myc 3′-UTR A region, which are proximal to the HuR-binding site in the B region. The FMTRIPs are not complementary to any native mRNA in Vero cells.

In cells transfected with c-Myc A, we observed no PLA signal between c-Myc and HuR (Figure 4). When HuR was increased by transfecting cells with both c-Myc A and HuR-GFP, there was a small increase in the mean PLA frequency, likely due to increased random interactions between c-Myc and HuR (Figure 4B; Supplementary Tables S1 and S2). In contrast, c-Myc AB transfection resulted in PLA signal between c-Myc and HuR (Figure 4A). The difference in the mean PLA frequency between c-Myc A and c-Myc AB transfected cells was significant (Figure 4B; Supplementary Tables S1 and S2). With HuR-GFP transfection, the frequency of interactions between c-Myc AB and HuR increased slightly (Figure 4B; Supplementary Tables S1 and S2).

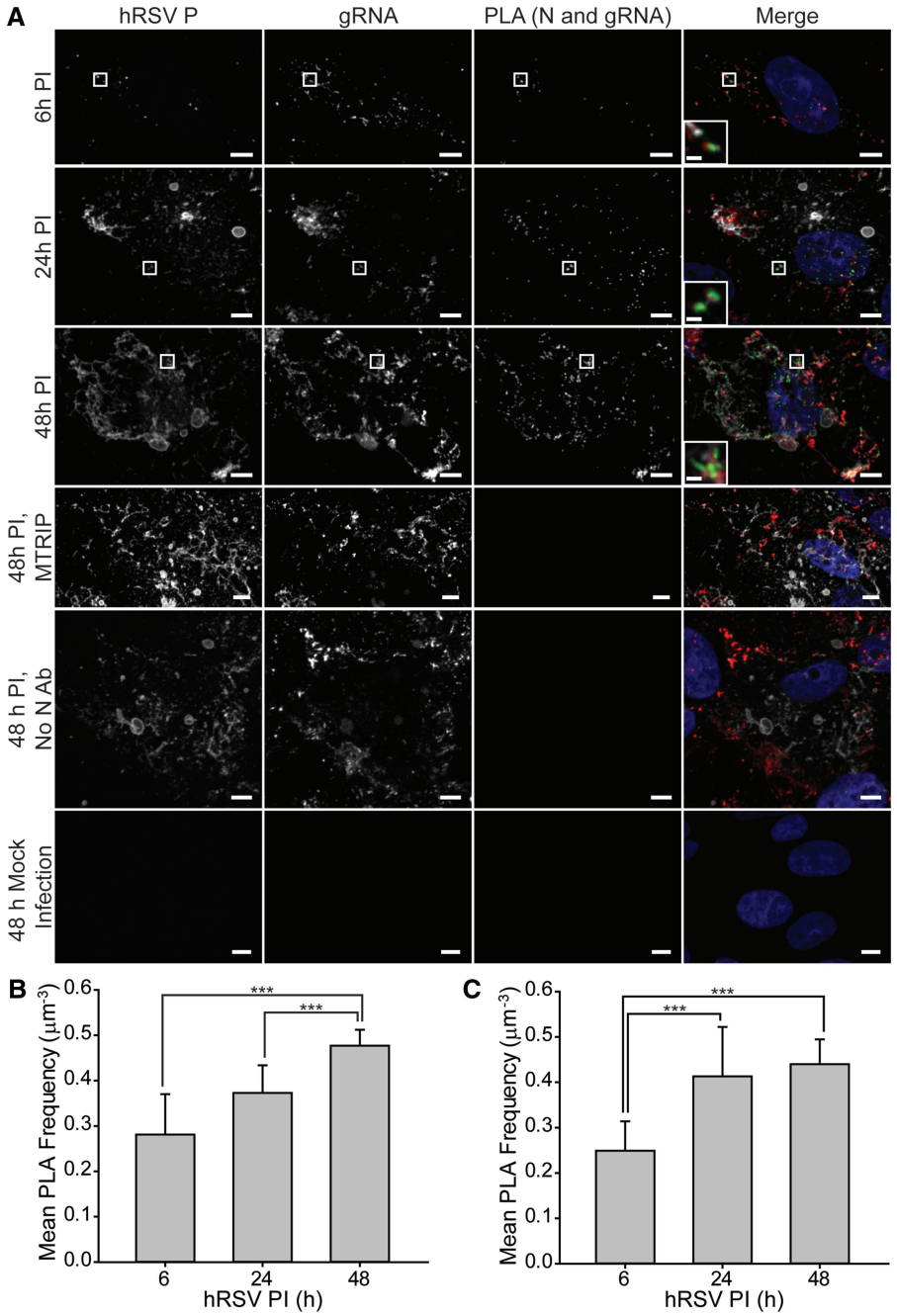

Figure 3. Imaging and quantification of PLA between hRSV N and gRNA 6, 24 and 48 h PI. (**A**) hRSV P protein IF, gRNA and PLA between N and gRNA in Vero cells 6, 24 and 48 h PI were imaged with a laser-scanning confocal microscope. Vero cells with untagged MTRIP, anti-N antibody omitted and mock infection served as negative controls. Merged images of RSV P (white), gRNA (red), PLA (green) and nuclei (blue) are shown. All image planes are represented. Inset, images of boxed regions. Scale bar, 5 µm (1 µm in insets). (**B**) The mean PLA frequency in Vero cells increased from 6 ($n = 14$, mean = 0.28, SD = 0.09), 24 ($n = 14$, mean = 0.37, SD = 0.06) and 48 h PI ($n = 14$, mean = 0.48, SD = 0.04). $^{***}P < 0.001$ (one-way ANOVA with Tukey method). (**C**) The mean PLA frequency in A549 cells increased from 6 ($n = 14$, mean = 0.25, SD = 0.07), 24 ($n = 14$, mean = 0.41, SD = 0.11) and 48 h PI ($n = 14$, mean = 0.44, SD = 0.06). $^{***}P < 0.001$ (one-way ANOVA with Tukey method). Error bars,standard deviation.

HuR–mRNA interactions increase with HuR overexpression and actD exposure

In order to investigate this technique's capacity to detect native mRNA–protein interactions, we compared interactions between HuR and two mRNA sequences, poly(A) (17) and the β-actin 3′-UTR (18), in HeLa cells, with and without HuR-GFP transfection, and when exposed to actD. Although predominately localized within the nucleus, HuR has been shown to increase its cytoplasmic concentration during actD exposure and to stabilize mRNAs by binding to them (27,28). We used PLA to examine changes in the HuR–mRNA interactions

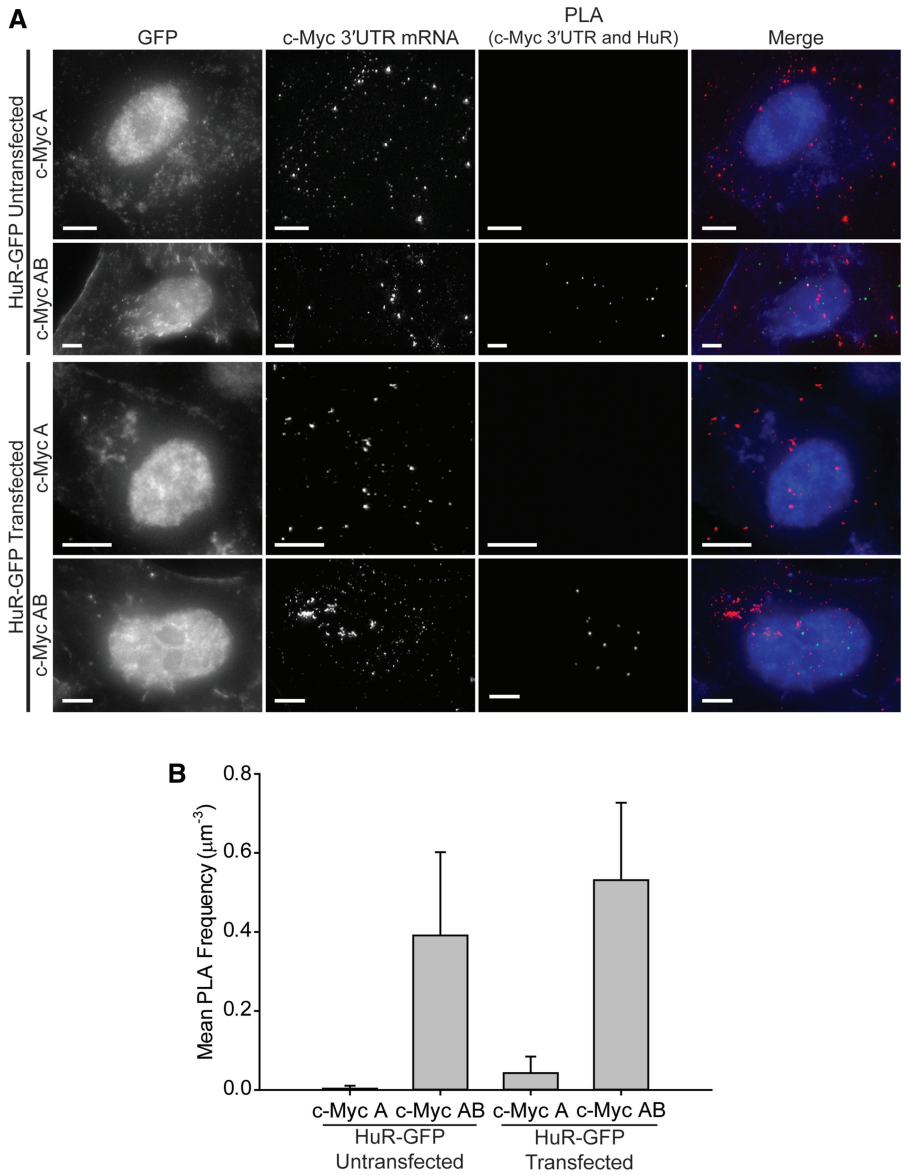

Figure 4. Imaging and quantification of PLA between HuR and c-Myc 3′-UTR mRNA containing the HuR-binding site (c-Myc AB) or lacking it (c-Myc A) in Vero cells with varying levels of HuR. (**A**) GFP IF, c-Myc 3′-UTR mRNA, PLA between c-Myc 3′-UTR and HuR were imaged in untransfected and HuR-GFP transfected Vero cells co-transfected with either GFP-c-Myc A or GFP-c-Myc AB. Merged images of GFP IF (blue), c-Myc 3′-UTR mRNA (red) and PLA (green) are shown. All the images were deconvolved, except for GFP and PLA. All image planes are represented. Scale bar: 5 μm. (**B**) The mean PLA frequency was minimal in cells transfected with c-Myc A, lacking the HuR-binding site. It was significantly greater in the presence of HuR-binding site with c-Myc AB transfection. (Supplementary Table S1 for two-way ANOVA with Holm–Sidak method and Supplementary Table S2 for Kruskal–Wallis one-way ANOVA with Dunn's method for multiple comparisons) Error bars, SD.

upon HuR overexpression and increased cytosolic localization, during actD-triggered transcription inhibition (29). After 36 h of transfection with HuR-GFP, FMTRIPs were delivered to cells using SLO. After 15 min, the cells were exposed to actD and fixed at specified times. Although increasing the number of MTRIPs targeting different sites on β-actin mRNA has been shown to increase the average fluorescence intensity of the mRNA-bound probe signal (18), no difference in the mean PLA frequency was observed in cells with three FMTRIPs targeting the coding region of β-actin mRNA, three targeting the 3′-UTR or all six (Supplementary Figure S9). Hence, PLA likely detected the occurrence of single interaction between a HuR and the closest FMTRIP bound to β-actin mRNA; therefore, the presence of additional probes on the mRNA does not increase the number of detected interactions.

In addition to the variability in transfection efficiency, which contributed to varying amounts of HuR, we observed cell-to-cell variability in mRNA amount (Figure 5B–D) and HuR–mRNA interactions as measured by PLA signal (Supplementary Figure S10). It is important to note that because the difference between the nuclear and cytoplasmic concentrations of HuR is beyond the imageable dynamic range using immunofluorescence (27,28), the cytoplasmic HuR fraction could not

be imaged without saturating the nuclear signal. Hence, even though HuR may not be observable in the photomicrographs, PLA occurred in the cytoplasm where HuR and mRNA interact (Figures 5–7) due to the greater sensitivity of PLA. In addition, in order to produce meaningful statistical data, for each transfection condition, we analysed only the cells expressing similar levels of nuclear HuR as measured using the mean IF intensity (600–1000 a.u.). It should also be noted that the concentration of poly(A) FMTRIPs used (60 nM) was less than the concentration that resulted in the maximum intensity (90 nM). By under-sampling, we were able to label a random portion of the mRNA population, which facilitated the imaging of individual granules and detection of relative changes in HuR interactions. β-actin FMTRIPs were delivered at a concentration (20nM for each of three FMTRIPs) such that they bind to >80% of the β-actin mRNA (18).

First, we quantified how the mRNA signal varied under our experimental conditions. Under normal growth conditions, cytoplasmic mRNA, as detected using poly(A) FMTRIPs, were found to be more abundant in untransfected HeLa cells than in the transfected ones (Figure 5B and Supplementary Table S3). The large, observed standard deviation was likely due to the heterogeneity in the population. Wheras HuR overexpression did not increase the overall cytoplasmic mRNA amount, we found that it dramatically slowed the effect of actD in reducing mRNA number, after 30 min of exposure. (Figure 5B; Supplementary Table S3 and S4). ActD treatment on HuR-transfected cells had more dramatic effects on β-actin mRNA, both as detected by using 3′-UTR FMTRIPs and analysed by qRT–PCR. HuR overexpression stabilized the β-actin mRNA and increased its quantity in the cytoplasm, consistent with the findings by Dormoy-Raclet *et al.* (25) (Figure 5C and D; Supplementary Tables S6–S11). With 60 min exposure to actD, the β-actin mRNA decreased to similar levels in transfected and untransfected cells.

In order to demonstrate the specificity and sensitivity of PLA, we compared PLA signal in cells containing untargeted or targeted FMTRIPs (Figure 6B and Supplementary Figure S11B) and with varying levels of HuR (Figure 6B and Supplementary Figure S11). In cells with untargeted probes, the PLA signal was minimal (Figure 6B; Supplementary Figure S11B and Supplementary Tables S10–S14). However, in HuR-GFP transfected cells with increased levels of HuR, the mean PLA frequency increased to a level similar to the untransfected cells with poly(A) FMTRIPs, but significantly less than the HuR-GFP transfected cells delivered poly(A) FMTRIPs (Figure 6B and Supplementary Tables S10–S14). This was likely due to increased random interactions between FMTRIP and HuR with a greater amount of HuR in the cytoplasm. When the HuR level was decreased using HuR siRNA, the PLA signal fell to a minimal level, similar to the untransfected cells containing untargeted probes (Figure 6B; Supplementary Figure S11A and Supplementary Tables S10–S14). In contrast, in cells transfected with a control siRNA that had no effect on HuR, the mean PLA frequency was similar to that of the untransfected cells delivered poly(A) FMTRIPs (Figure 6B; Supplementary Figure S11A and Supplementary Tables S10–S14). Here, we showed that PLA specifically detected interactions between the poly(A)+ mRNA and HuR. The mean PLA frequency quantifiably demonstrated changes in the frequency of interactions between mRNA and HuR, as the amount of HuR decreased and increased.

Next, given that actD exposure has been shown to increase HuR binding to mRNA in the cytoplasm (28), we quantified the HuR–mRNA interactions via PLA but selected cells with a similar range of FMTRIP signal volume (poly(A), $60 \pm 40\,\mu m^3$; β-actin, $160 \pm 90\,\mu m^3$). The mean PLA frequency increased with HuR overexpression and longer exposure to actD (Figures 6A, C and 7; Supplementary Figures S12 and S13). Specifically, in transfected cells and in the absence of actD, the frequency of HuR interactions increased 99% with poly(A)+ mRNA (Figure 6C) and 255% with β-actin mRNA (Figure 7B) greater than in untransfected cells. In transfected cells and in the presence of actD, the frequency of HuR interactions increased 184% with poly(A)+ mRNA (Figure 6C) and 250% with β-actin mRNA (Figure 7B). No PLA was observed in transfected, MTRIP-delivered (no flag tag) cells (Figure 6A). Although these changes in mRNA stability and interactions resulting from changes in HuR localization may seem less than those reported using UV-cross-linking (33,34) and gel shift assay (28), our findings show changes in individual cells, not in cell lysates.

DISCUSSION

In this study, we demonstrated that native RNA–protein interactions can be imaged and quantified *in situ* at the single-interaction level using flag-tagged MTRIPs and proximity ligation. We described the progression of an hRSV infection in Vero and A549 cells and the associated increase in the interactions between the viral gRNA and nucleocapsid protein. We also showed heterogeneous fluctuations in endogeneous mRNAs and RNA–protein interactions. We imaged and quantified these changes due to altered HuR levels, via transfection, and HuR localization, via actD exposure, and the resulting variation in poly(A)+ and β-actin mRNA expression, which was confirmed with qRT–PCR. Unlike other imaging approaches, such as FRET and FC, PLA detected and quantified these changes at the single interaction level (16). It also targeted specific RNA sequences and RBPs at their native levels (15). Compared with co-localization analysis, this method detected interactions between two signals with disparate dynamic ranges. For example, although the FMTRIP intensity was within the detectable range throughout the cell, the intensity of nuclear HuR IF was so high that the cytoplasmic signal could not be imaged without oversaturating the nuclear signal. Hence, the co-localization between FMTRIP and HuR IF could not be detected in the cytoplasm without omitting the nucleus. PLA solved this problem by producing fluorescent punctae with uniform intensity that fell within the detectable range.

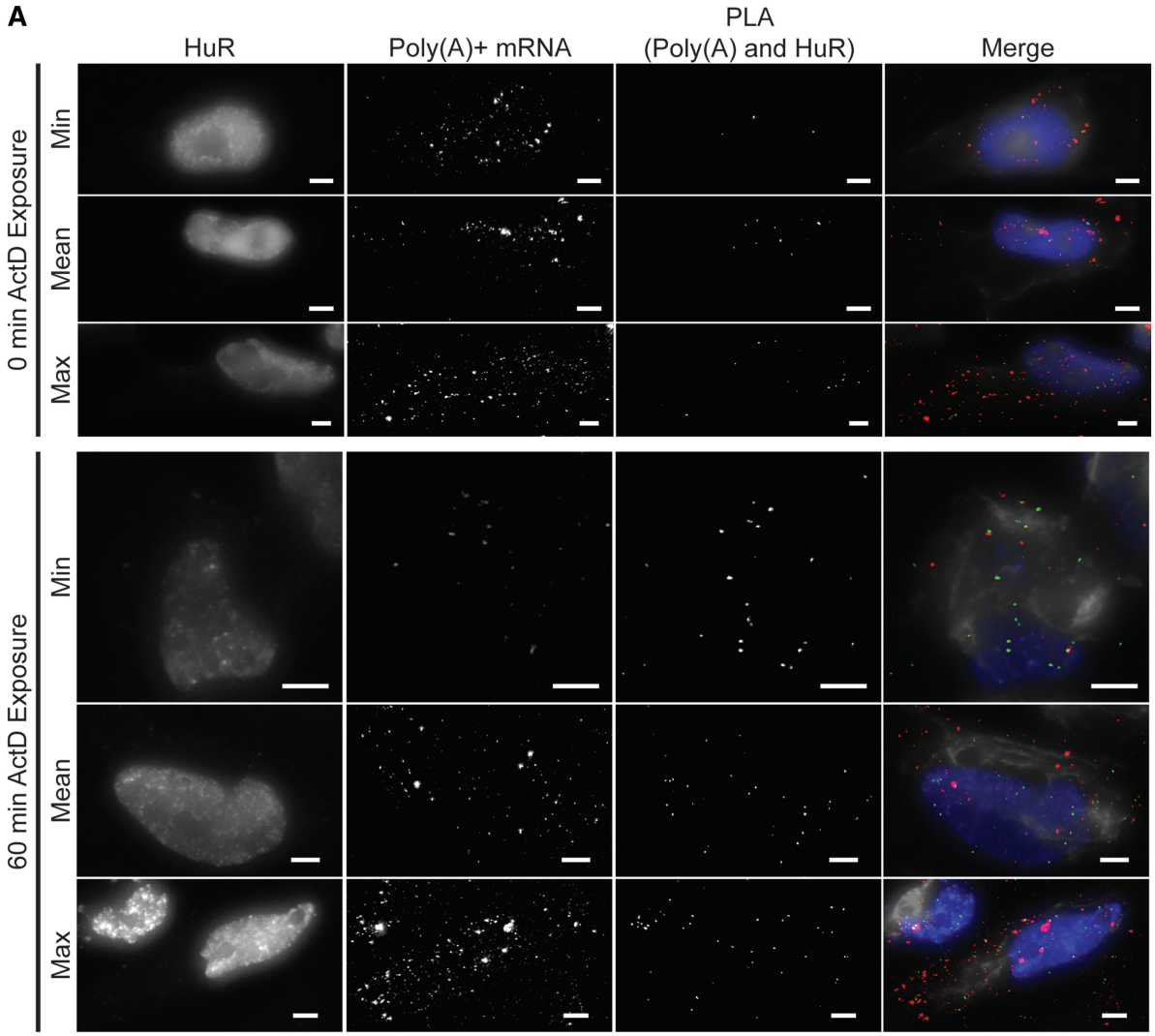

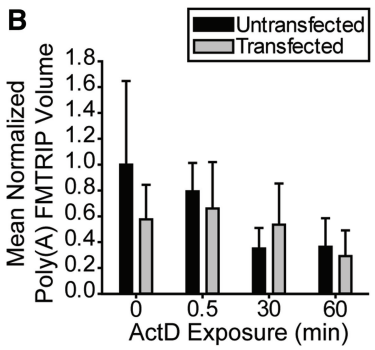

C

		ActD Exposure (min)	Mean ± s.d. (n)
Normalized β-actin 3'UTR FMTRIP Volume	Untransfected	0	1.0 ± 1.3 (24)
		60	0.4 ± 0.2 (33)
	Transfected	0	14.4 ± 14.4 (19)
		60	0.3 ± 0.2 (25)

D

		ActD Exposure (min)	RQ (minimum, maximum RQ)
RQ β-actin cytoplasmic mRNA	Untransfected	0	1.0 (0.8, 1.2)
		60	1.0 (0.8,1.2)
	Transfected	0	1.3 (1.1, 1.5)
		60	0.8 (0.6, 1.0)

Figure 5. Imaging and quantification of cell-to-cell variability in poly(A)+ and β-actin mRNA. (**A**) HuR IF, poly(A)+ mRNA, PLA between poly(A) and HuR were imaged in transfected HeLa cells with the mean HuR IF intensity and volume within 1 SD after 0 and 60 min actD exposure. Those with the minimum (min), mean and maximum (max) mRNA volume and PLA frequency imaged using a widefield microscope are shown. Merged images of vimentin IF (white), poly(A)+ mRNA (red), PLA (green) and HuR IF (blue) are shown. All the images were deconvolved, except for HuR and vimentin IF. All image planes are represented. Scale bar, 5 μm. (**B**) Comparison of the mean normalized poly(A) FMTRIP volume in HuR-GFP transfected and untransfected HeLa cells exposed to actD for 0–60 min. The values were normalized to the mean of untransfected cells with 0 min actD exposure. FMTRIP volume decreased with longer actD (5 μg/ml) exposure. (Supplementary Tables S3–S5 for two-way ANOVA with Holm–Sidak method) (**C**) Comparison of the mean normalized β-actin 3′-UTR FMTRIP volume in HuR-GFP transfected and untransfected HeLa cells exposed to actD for 0 and 60 min. The values were normalized to the mean of untransfected cells with 0 min actD exposure. Generally, FMTRIP volume decreased with longer actD exposure. Without actD, the mean FMTRIP volume in transfected cells was significantly greater than that of untransfected cells. (Supplementary Tables S6–S8 for two-way ANOVA with Holm–Sidak method) (**D**) Comparison of the RQ of β-actin cytoplasmic mRNA determined using qRT–PCR of RNA collected from HuR-GFP transfected and untransfected HeLa cells exposed to actD for 0 and 60 min. (Supplementary Tables S9–S11 for two-way ANOVA with Bonferroni *post-hoc* method).

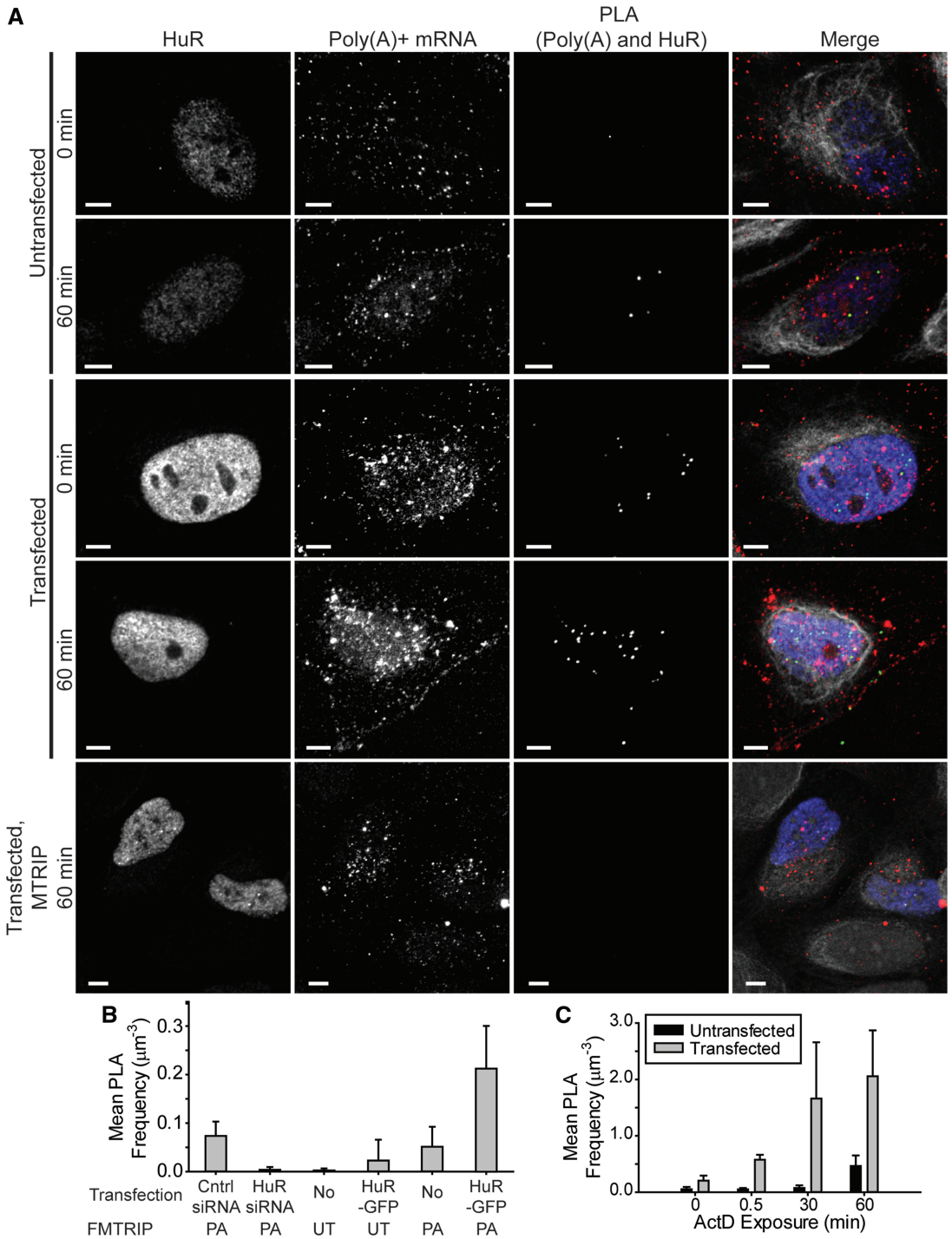

Figure 6. Imaging and quantification of interactions between HuR and poly(A)+ mRNA in HuR-GFP transfected and untransfected HeLa cells exposed to actD for 0–60 min. (**A**) HuR IF, poly(A)+ mRNA, PLA between Poly(A) and HuR were imaged in untransfected and transfected HeLa cells exposed to actD for 0 and 60 min, using a laser-scanning confocal microscope. Untagged-MTRIP delivered transfected cells after 60 min actD exposure are shown as a negative control. Merged images of vimentin IF (white), poly(A)+ mRNA (red), PLA (green) and HuR IF (blue) are shown. All image planes are represented. Scale bar, 5 μm. (**B**) The mean HuR-poly(A) PLA frequency in HeLa cells transfected with 200 nM HuR siRNA (Transfection = HuR siRNA, MTRIP = PA) was minimal, whereas it was similar in cells transfected with 200 nM control siRNA (Transfection = control siRNA, MTRIP = PA) and the untransfected cells (Transfection = No, MTRIP = PA). In cell-delivered untargeted MTRIPs (UT), the mean HuR-UT PLA frequency (Transfection = No, MTRIP = UT) was minimal. With HuR-GFP transfection (Transfection = HuR-GFP, MTRIP = UT), it increased but remained less than the mean HuR-poly(A) PLA frequency of untransfected (Transfection = No, MTRIP = PA) and transfected (Transfection = HuR-GFP, MTRIP = PA) cells. (Supplementary Tables S12–S16) (**C**) The mean HuR-poly(A) PLA frequency increased with longer exposure to actD (5 μg/ml) in untransfected and transfected HeLa cells. (Supplementary Tables S17–S19 for two-way ANOVA with Holm–Sidak method) Error bars, standard deviation.

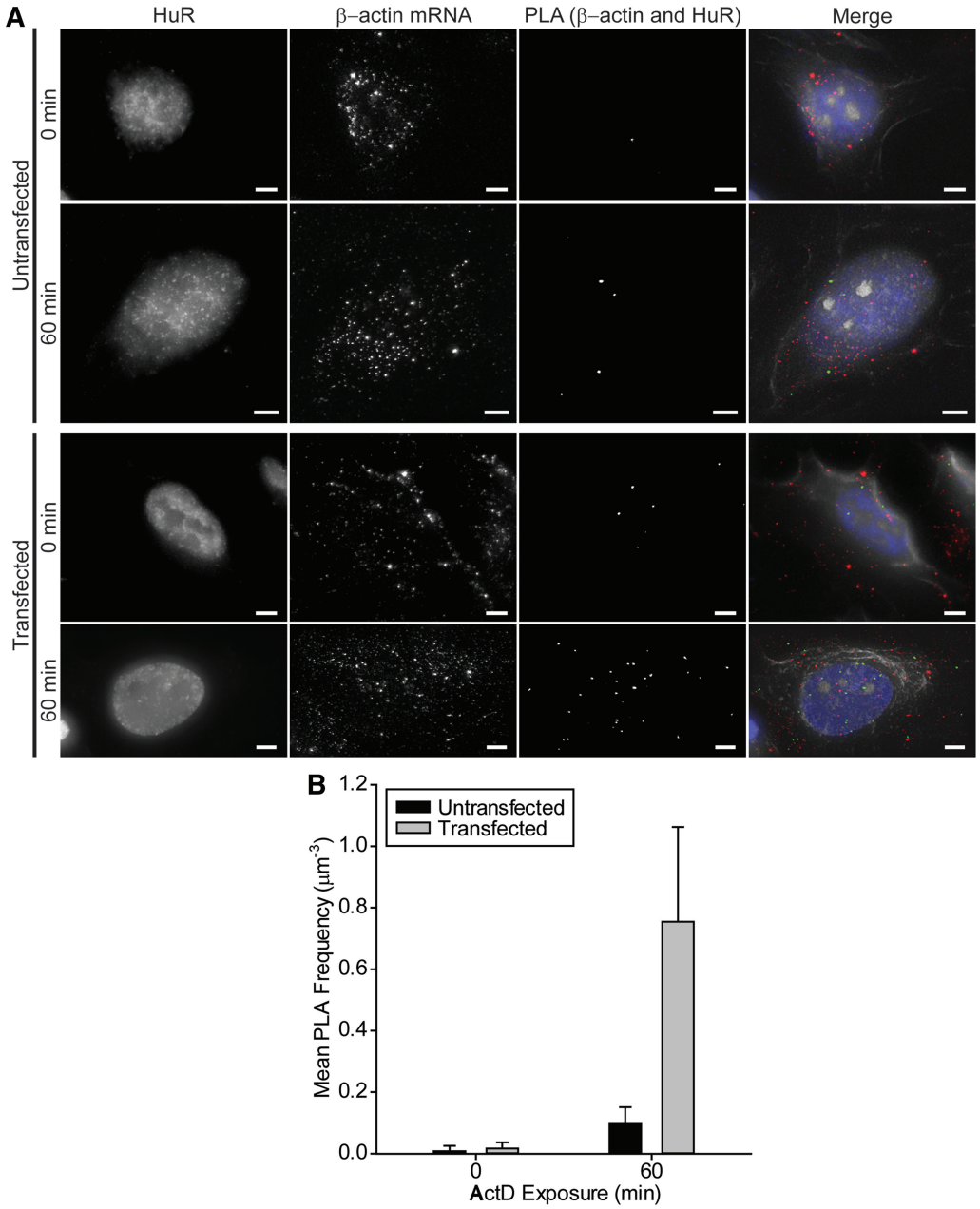

Figure 7. Imaging and quantification of interactions between HuR and β-actin 3′-UTR in HuR-GFP transfected and untransfected HeLa cells exposed to actD for 0 and 60 min. (**A**) HuR IF, β-actin mRNA and PLA between β-actin 3′-UTR and HuR were imaged in untransfected and transfected HeLa cells exposed to actD for 0 and 60 min, using a widefield microscope. Merged images of vimentin IF (white), β-actin mRNA (red), PLA (green) and HuR IF (blue) are shown. The images have been deconvolved, except for HuR and vimentin IF. Scale bar, 5 μm. (**B**) The mean HuR-β-actin 3′-UTR PLA frequency increased with longer exposure to actD in untransfected and transfected HeLa cells. (Supplementary Tables S20–S22 for two-way ANOVA test with Holm–Sidak method) Error bars, standard deviation.

This method also offered many advantages over other biochemical techniques, such as immunoprecipitation assays, as it provided quantitative, spatial information *in situ*. We could select accurately for a specific signal by identifying the PLA signal co-localized with FMTRIP and protein IF. This method could be used to quantify RNA–protein interactions on a per cell basis, detecting the cell-to-cell variability within a cell population and its changes due to external stimuli. Although this method successfully quantifies relative changes in the frequency of interactions, it likely does not detect all the interactions or provide the absolute number of interactions. It is currently optimized to detect interactions between two molecules that are <40 nm apart (16). Weaker interactions might not be detected. However, this approach can be modified to detect interactions >40 nm or <10 nm by adjusting the length of oligonucleotide connectors (16). In addition, this technique can be adapted for multiplexing (35) by using different pairs of PLA probes and spectrally-distinct, fluorescently-labelled oligonucleotides.

Single-cell heterogeneity in cell populations has been widely observed (36–38). A deeper understanding of cellular processes can be gained from investigating this variation in both space and time on a per cell basis (39). Addressing this challenge is impossible with current biochemical techniques and difficult with imaging tools (40). Although an averaged view of the interaction network may provide valuable information, the spatiotemporal and cell-to-cell variation of RNA–protein interactions are important for investigating their role in a variety of cellular events, such as distinguishing early and late stages of infection in viral pathogenesis or identifying oncogenic, aberrant RNA–protein interactions that precede the synthesis of cancer-causing proteins among a heterogeneous population of cancerous and healthy cells. The FMTRIP-based PLA method is a powerful tool that meets this challenge. It provides accurate, easily detectable, quantifiable spatiotemporal information from which causal inference and hypothesis-driven statistics can be derived about the post-transcriptional regulation of RNA. This technique allows collection of large, high-throughput data that are necessary for mapping the RNA–protein interactome *in situ* and for rapid identification of interactions between a series of RNA sequences and their potential RBPs. It has potential to serve as a valuable diagnostic tool for disorders involving abnormal post-transcriptional regulations.

SUPPLEMENTARY DATA

Supplementary Data are available at NAR Online: Supplementary Tables 1–23 and Supplementary Figures 1–19.

ACKNOWLEDGEMENTS

The authors thank Drs Kyle Mansfield, Jack Keene and Imed Gallouzi for their informative correspondence, Dr Myriam Gorospe for supplying the HuR-GFP and c-Myc 3′-UTR plasmids and Dr James E. Crowe Jr. for supplying the mouse anti-hRSV P antibody and N-GFP plasmid. We also acknowledge the Institute of Bioengineering and Biosciences at Georgia Tech for use of the LSM 510 confocal microscope.

FUNDING

The National Institutes of Health (NIH) [CA147922, GM094198 to P.J.S.]. Funding for open access charge: NIH.

Conflict of interest statement. None declared.

REFERENCES

1. Black,D.L. (2003) Mechanisms of alternative pre-messenger RNA splicing. *Annu. Rev. Biochem.*, **72**, 291–336.
2. Chen,C.-Y. and Shyu,A. (1995) AU-rich elements - characterization and importance in messenger-RNA degradation. *Trends Biochem. Sci.*, **20**, 465–470.
3. Martin,K.C. and Ephrussi,A. (2009) mRNA localization: gene expression in the spatial dimension. *Cell*, **136**, 719–730.
4. Sonenberg,N. and Hinnesbusch,A.G. (2008) Regulation of translation initiation in eukaryotes: mechanisms and biological targets. *Cell*, **136**, 731–745.
5. Shapira,S.D., Gat-Viks,I., Shum,B.O.V., Dricot,A., Degrace,M., Liguo,W., Gupta,P.B., Hao,T., Silver,S.J., Root,D.E. *et al.* (2009) A physial and regulatory map of host-influenza interactions reveal pathways in H1N1 infection. *Cell*, **139**, 1255–1267.
6. Culbertson,M.R. (1999) RNA surveillance: unforseen consequences for gene expression, inherited genetic disorders and cancer. *Trends Genet.*, **15**, 74–80.
7. van Kouwenhove,M., Kedde,M. and Agami,R. (2011) MicroRNA regulation by RNA-binding proteins and its implications for cancer. *Nat. Rev. Cancer*, **11**, 644–656.
8. Adeli,K. (2011) Translational control mechanisms in metabolic regulation: critical role of RNA binding proteins, microRNAs, and cytoplasmic RNA granules. *Am. J. Physiol. Endocrinol. Metab.*, **301**, E1051–E1064.
9. Hogan,D.J., Riordan,D.P., Gerber,A.P., Herschlag,D. and Brown,P.O. (2008) Diverse RNA-binding proteins interact with functionally related sets of RNAs, suggesting an extensive regulatory system. *PLoS Biol.*, **6**, e255.
10. Rodriguez,A.J., Czaplinski,K., Condeelis,J.S. and Singer,R.H. (2008) Mechanisms and cellular roles of local protein synthesis in mammalian cells. *Curr. Opin. Cell Biol.*, **20**, 144–149.
11. Kaern,M., Elston,T.C., Blake,W.J. and Collins,J.J. (2005) Stochasticity in gene expression: from theories to phenotypes. *Nat. Rev. Genet.*, **6**, 451–464.
12. Huranova,M., Jablonski,J.A., Benda,A., Hof,M., Stanek,D. and Caputi,M. (2009) In vivo detection of RNA-binding protein interactions with cognate RNA sequences by fluorescence resonance energy transfer. *RNA*, **15**, 2063–2071.
13. Lorenz,M. (2009) Visualizing protein-RNA interactions inside cells by fluorescence resonance energy tranfer. *RNA*, **15**, 97–103.
14. Rackham,O. and Brown,C.M. (2004) Visualization of RNA-protein interactions in living cells: FMRP and IMP1 interact on mRNAs. *EMBO J.*, **23**, 3346–3355.
15. Santangelo,P.J., Lifland,A.W., Curt,P., Sasaki,Y., Bassell,G.J., Lindquist,M.E. and Crowe,J.E. Jr (2009) Single molecule-sensitive probes for imaging RNA in live cells. *Nat. Methods*, **6**, 347–349.
16. Soderberg,O., Gulberg,M., Jarvius,M., Ridderstrale,K., Leuchowius,K., Jarvius,J., Wester,K., Hydbring,P., Bahram,F., Larsson,L. *et al.* (2006) Direct observation of individual endogenous protein complexes in situ by proximity ligation. *Nat. Methods*, **3**, 995–1000.
17. Zurla,C., Lifland,A.W. and Santangelo,P.J. (2011) Characterizing mRNA interactions with RNA granules during translation initiation inhibition. *PLoS One*, **6**, e19727.
18. Lifland,A.W., Zurla,C., Yu,J. and Santangelo,P.J. (2011) Dynamics of native b-actin mRNA transport in the cytoplasm. *Traffic*, **12**, 1000–1011.
19. Lal,A., Kawai,T., Yang,X., Mazan-Mamczarz,K. and Gorospe,M. (2005) Antiapoptotic function of RNA-binding protein HuR effected through prothymosin. *EMBO J.*, **25**, 1852–1862.
20. Mazan-Mamczarz,K., Hagner,P.R., Corl,S., Srikantan,S., Wood,W.H., Becker,K.G., Gorospe,M., Keene,J.D., Levenson,A.S. and Gartenhaus,R.B. (2008) Post-transcriptional gene regulation by HuR promotes a more tumorigenic phenotype. *Oncogene*, **27**, 6151–6163.
21. Yeap,B., Voon,D.C., Vivian,J.P., McCulloch,R.K., Thomson,A.M., Giles,K.M., Czyzyk-Krzeska,M.F., Furneaux,H., Wilce,M.C.J., Wilce,J.A. *et al.* (2002) Novel binding of HuR and poly(C)-binding protein to a conserved UC-rich motif withint the 3'-untranslated region of the androgen receptor messenger RNA. *J. Biol. Chem.*, **277**, 27183–27192.
22. Ma,W.-J., Chung,S. and Furneaux,H. (1997) The Elav-like proteins bind to AU-rich elements and to the poly(A) tail of mRNA. *Nucleic Acids Res.*, **25**, 3564–3569.
23. Mistuitta,C.M., Iyer,V.R., Werstiuk,E.S. and Grover,A.K. (2001) The role of 3'-untranslated region (3'-UTR) mediated mRNA stability in cardiovascular pathophysiology. *Mol. Cell. Biochem.*, **224**, 53–67.

24. de Silanes,L., Quesada,M.P. and Esteller,M. (2007) Aberrant regulation of messenger RNA 3'-untranslated region in human cancer. *Cell. Oncol.*, **29**, 1–17.
25. Dormoy-Raclet,V., Menard,I., Clair,E., Kurban,G., Mazroui,R., Di Marco,S., von Roretz,C., Pause,A. and Gallouzi,I. (2007) The RNA-binding protein HuR promotes cell migration and cell invasion by stabilizing the b-actin mRNA in a U-rich-element-dependent manner. *Mol. Cell. Biol.*, **27**, 5365–5380.
26. Fan,X.C. and Steitz,J.A. (1998) HNS, a nuclear-cytoplasmic shuttling sequence in HuR. *Proc. Natl Acad. Sci. USA*, **95**, 15293–15298.
27. Fan,X.C. and Steitz,J.A. (1998) Overexpression of HuR, a nuclear-cytoplasmic shuttling protein, increases the in vivo stability of ARE-containing mRNAs. *EMBO J.*, **17**, 3448–3460.
28. Peng,S.S.Y., Chen,C.A., XuN. and Shyu,A. (1998) RNA stabilization by the AU-rich element binding protein, HuR, an ELAV protein. *EMBO J.*, **17**, 3461–3470.
29. Nakazato,H., Edmonds,M. and Kopp,D.W. (1974) Differential metabolism of large and small poly(A) sequences in the heterogeneous nuclear RNA of HeLa cells. *PNAS*, **71**, 200–204.
30. Schmittgen,T.D. and Livak,K.J. (2008) Analyzing real-time PCR data by the comparative CT method. *Nat. Protoc.*, **3**, 1101–1108.
31. Collins,P.L. and Crowe,J.E. Jr (2007) *Fields Virology*, 5th edn. Lippincott Williams & Wilkins, Philadelphia, PA.
32. Kim,H.H., Kuwano,Y., Srikantan,S., Lee,E.K., Martindale,J.L. and Gorospe,M. (2009) HuR recruits let-7/RISC to repress c-Myc expression. *Genes Dev.*, **23**, 1743–1748.
33. Mukherjee,N., Corcoran,D.L., Nusbaum,J.D., Reid,D.W., Georgiev,S., Hafner,M., Ascano,M. Jr, Tuschl,T., Ohler,U. and Keene,J.D. (2011) Integrative regulatory mapping indicates that the RNA-binding protein HuR couples pre-mRNA processing and mRNA stability. *Mol. Cell*, **43**, 327–339.
34. Lebedeva,S., Jens,M., Theil,K., Schwanhausser,B., Selbach,M., Landthaler,M. and Rejewsky,N. (2011) Transcriptome-wide analysis of regulatory interactions of the RNA-binding protein HuR. *Mol. Cell*, **43**, 340–352.
35. Fredriksson,S., Dixon,W., Ji,H., Koong,A., Mindrinos,M. and Davis,R.W. (2007) Multiplexed protein detection by proximity ligation for cancer biomarker validation. *Nat. Methods*, **4**, 327–329.
36. Snijder,B., Sacher,R., Ramo,P., Damm,E., Liberali,P. and Pelkmans,L. (2009) Poulation context determines cell-to-cell variability in endocytosis and virus infection. *Nat. Protoc.*, **461**, 520–523.
37. Raj,A. and van Oudenaarden,A. (2008) Nature, nurture, or chance: stochastic gene expression and its consequences. *Cell*, **135**, 216–226.
38. Levsky,J.M. and Singer,R.H. (2003) Gene expression and the myth of the average cell. *Trends Cell Biol.*, **13**, 4–6.
39. Pelkmans,L. (2012) Using cell-to-cell variablity-a new ear in molecular biology. *Science*, **336**, 425–426.
40. Welch,C.M., Elliott,H., Danuser,G. and Hahn,K.M. (2011) Imaging the coordination of multiple signalling activities in living cells. *Nat. Rev. Mol. Cell Biol.*, **12**, 749–756.